ARTICLES

Measurements of R_b with impact parameters and displaced vertices

K. Abe,[29] I. Abt,[14] C.J. Ahn,[26] T. Akagi,[27] N.J. Allen,[4] W.W. Ash,[27,*] D. Aston,[27] K.G. Baird,[24] C. Baltay,[33] H.R. Band,[32] M.B. Barakat,[33] G. Baranko,[10] O. Bardon,[16] T. Barklow,[27] A.O. Bazarko,[11] R. Ben-David,[33] A.C. Benvenuti,[2] T. Bienz,[27] G.M. Bilei,[22] D. Bisello,[21] G. Blaylock,[7] J.R. Bogart,[27] T. Bolton,[11] G.R. Bower,[27] J.E. Brau,[20] M. Breidenbach,[27] W.M. Bugg,[28] D. Burke,[27] T.H. Burnett,[31] P.N. Burrows,[16] W. Busza,[16] A. Calcaterra,[13] D.O. Caldwell,[6] D. Calloway,[27] B. Camanzi,[12] M. Carpinelli,[23] R. Cassell,[27] R. Castaldi,[23,†] A. Castro,[21] M. Cavalli-Sforza,[7] E. Church,[31] H.O. Cohn,[28] J.A. Coller,[3] V. Cook,[31] R. Cotton,[4] R.F. Cowan,[16] D.G. Coyne,[7] A. D'Oliveira,[8] C.J.S. Damerell,[25] M. Daoudi,[27] R. De Sangro,[13] P. De Simone,[13] R. Dell'Orso,[23] M. Dima,[9] P.Y.C. Du,[28] R. Dubois,[27] B.I. Eisenstein,[14] R. Elia,[27] E. Etzion,[4] D. Falciai,[22] M.J. Fero,[16] R. Frey,[20] K. Furuno,[20] T. Gillman,[25] G. Gladding,[14] S. Gonzalez,[16] G.D. Hallewell,[27] E.L. Hart,[28] Y. Hasegawa,[29] S. Hedges,[4] S.S. Hertzbach,[17] M.D. Hildreth,[27] J. Huber,[20] M.E. Huffer,[27] E.W. Hughes,[27] H. Hwang,[20] Y. Iwasaki,[29] D.J. Jackson,[25] P. Jacques,[24] J. Jaros,[27] A.S. Johnson,[3] J.R. Johnson,[32] R.A. Johnson,[8] T. Junk,[27] R. Kajikawa,[19] M. Kalelkar,[24] H. J. Kang,[26] I. Karliner,[14] H. Kawahara,[27] H.W. Kendall,[16] Y. Kim,[26] M.E. King,[27] R. King,[27] R.R. Kofler,[17] N.M. Krishna,[10] R.S. Kroeger,[18] J.F. Labs,[27] M. Langston,[20] A. Lath,[16] J.A. Lauber,[10] D.W.G. Leith,[27] M.X. Liu,[33] X. Liu,[7] M. Loreti,[21] A. Lu,[6] H.L. Lynch,[27] J. Ma,[31] G. Mancinelli,[22] S. Manly,[33] G. Mantovani,[22] T.W. Markiewicz,[27] T. Maruyama,[27] R. Massetti,[22] H. Masuda,[27] E. Mazzucato,[12] A.K. McKemey,[4] B.T. Meadows,[8] R. Messner,[27] P.M. Mockett,[31] K.C. Moffeit,[27] B. Mours,[27] G. Müller,[27] D. Muller,[27] T. Nagamine,[27] U. Nauenberg,[10] H. Neal,[27] M. Nussbaum,[8] Y. Ohnishi,[19] L.S. Osborne,[16] R.S. Panvini,[30] H. Park,[20] T.J. Pavel,[27] I. Peruzzi,[13,‡] M. Piccolo,[13] L. Piemontese,[12] E. Pieroni,[23] K.T. Pitts,[20] R.J. Plano,[24] R. Prepost,[32] C.Y. Prescott,[27] G.D. Punkar,[27] J. Quigley,[16] B.N. Ratcliff,[27] T.W. Reeves,[30] J. Reidy,[18] P.E. Rensing,[27] L.S. Rochester,[27] J.E. Rothberg,[31] P.C. Rowson,[11] J.J. Russell,[27] O.H. Saxton,[27] S.F. Schaffner,[27] T. Schalk,[7] R.H. Schindler,[27] U. Schneekloth,[16] B.A. Schumm,[15] A. Seiden,[7] S. Sen,[33] V.V. Serbo,[32] M.H. Shaevitz,[11] J.T. Shank,[3] G. Shapiro,[15] S.L. Shapiro,[27] D.J. Sherden,[27] K.D. Shmakov,[28] C. Simopoulos,[27] N.B. Sinev,[20] S.R. Smith,[27] J.A. Snyder,[33] P. Stamer,[24] H. Steiner,[15] R. Steiner,[1] M.G. Strauss,[17] D. Su,[27] F. Suekane,[29] A. Sugiyama,[19] S. Suzuki,[19] M. Swartz,[27] A. Szumilo,[31] T. Takahashi,[27] F.E. Taylor,[16] E. Torrence,[16] J.D. Turk,[33] T. Usher,[27] J. Va'vra,[27] C. Vannini,[23] E. Vella,[27] J.P. Venuti,[30] R. Verdier,[16] P.G. Verdini,[23] S.R. Wagner,[27] A.P. Waite,[27] S.J. Watts,[4] A.W. Weidemann,[28] E.R. Weiss,[31] J.S. Whitaker,[3] S.L. White,[28] F.J. Wickens,[25] D.A. Williams,[7] D.C. Williams,[16] S.H. Williams,[27] S. Willocq,[33] R.J. Wilson,[9] W.J. Wisniewski,[5] M. Woods,[27] G.B. Word,[24] J. Wyss,[21] R.K. Yamamoto,[16] J.M. Yamartino,[16] X. Yang,[20] S.J. Yellin,[6] C.C. Young,[27] H. Yuta,[29] G. Zapalac,[32] R.W. Zdarko,[27] C. Zeitlin,[20] Z. Zhang,[16] and J. Zhou[20]

(SLD Collaboration)

[1] *Adelphi University, Garden City, New York 11530*
[2] *INFN, Sezione di Bologna, I-40126 Bologna, Italy*
[3] *Boston University, Boston, Massachusetts 02215*
[4] *Brunel University, Uxbridge, Middlesex UB8 3PH, United Kingdom*
[5] *California Institute of Technology, Pasadena, California 91125*
[6] *University of California at Santa Barbara, Santa Barbara, California 93106*
[7] *University of California at Santa Cruz, Santa Cruz, California 95064*
[8] *University of Cincinnati, Cincinnati, Ohio 45221*
[9] *Colorado State University, Fort Collins, Colorado 80523*
[10] *University of Colorado, Boulder, Colorado 80309*
[11] *Columbia University, New York, New York 10027*
[12] *INFN, Sezione di Ferrara and Università di Ferrara, I-44100 Ferrara, Italy*
[13] *INFN, Laboratori Nazionali di Frascati, I-00044 Frascati, Italy*
[14] *University of Illinois, Urbana, Illinois 61801*
[15] *Lawrence Berkeley Laboratory, University of California, Berkeley, California 94720*
[16] *Massachusetts Institute of Technology, Cambridge, Massachusetts 02139*
[17] *University of Massachusetts, Amherst, Massachusetts 01003*
[18] *University of Mississippi, University, Mississippi 38677*
[19] *Nagoya University, Chikusa-ku, Nagoya 464, Japan*
[20] *University of Oregon, Eugene, Oregon 97403*

*Deceased.
†Also at the Università di Genova, Genova, Italy.
‡Also at the Università di Perugia, Perugia, Italy.

0556-2821/96/53(3)/1023(16)/$06.00 ©1996 The American Physical Society

[21] INFN, Sezione di Padova and Università di Padova, I-35100 Padova, Italy
[22] INFN, Sezione di Perugia and Università di Perugia, I-06100 Perugia, Italy
[23] INFN, Sezione di Pisa and Università di Pisa, I-56100 Pisa, Italy
[24] Rutgers University, Piscataway, New Jersey 08855
[25] Rutherford Appleton Laboratory, Chilton, Didcot, Oxon OX11 0QX, United Kingdom
[26] Sogang University, Seoul, Korea
[27] Stanford Linear Accelerator Center, Stanford University, Stanford, California 94309
[28] University of Tennessee, Knoxville, Tennessee 37996
[29] Tohoku University, Sendai 980, Japan
[30] Vanderbilt University, Nashville, Tennessee 37235
[31] University of Washington, Seattle, Washington 98195
[32] University of Wisconsin, Madison, Wisconsin 53706
[33] Yale University, New Haven, Connecticut 06511
(Received 11 May 1995)

We present measurements of R_b using the SLD at the SLC. The analyses use 2D and 3D impact parameter tags and a displaced 3D vertex tag which all exploit the small size and stability of the e^+e^- interaction point and the precision 3D CCD pixel vertex detector to achieve high $b\bar{b}$-tagging efficiencies and purities. The combined measurement yields $R_b = 0.229 \pm 0.011$ and is consistent with standard model predictions.

PACS number(s): 13.38.Dg, 13.65.+i

I. INTRODUCTION

Measurements of the $Z^0 \to b\bar{b}$ coupling provide an interesting means for testing the standard model. In contrast with those for light flavors, the $Z^0 \to b\bar{b}$ vertex is expected to be subject to relatively large radiative corrections resulting from $|V_{tb}| \sim 1$ and the large top quark mass [1]. The quantity $R_b = \frac{\Gamma(Z^0 \to b\bar{b})}{\Gamma(Z^0 \to \text{hadrons})}$ isolates the $Z^0 \to b\bar{b}$ vertex corrections as it is insensitive to QCD effects and oblique corrections which affect all quark flavors equally. Using R_b, vertex corrections directly resulting from the presence of the t quark may be observed. Recent evidence from the Collider Detector at Fermilab (CDF) and D0 Collaborations for a top quark mass of $\sim 180\,\text{GeV}/c^2$ [2] suggests that a deviation in R_b from the tree level coupling of $\sim -1.8\%$ should be observed. Furthermore, proposed extensions of the standard model would imply additional potentially measurable deviations in R_b from the minimal standard model value [3]. Currently, the average R_b measurement at the CERN e^+e^- collider LEP is $\sim 2\sigma$ high [4] compared to the standard model value.

The R_b measurements are performed by applying cuts to event or hemisphere characteristics which distinguish the decay of a B hadron from others. This identification of b decays is called b tagging. A very pure b tag is desirable to reduce systematic uncertainties from simulation of non-b decays and a high b-tag efficiency is needed to reduce statistical uncertainties. The large mass and long lifetime (~ 1.5 ps) of B hadrons lead to decay signatures which uniquely distinguish them from charm and light quark decays. The LEP measurements utilize high p and p_t lepton tags [5], b tags on event shape variables [6], b tags on the hemispheres of an event that allow calibration of the b-tagging effiency from data [7], or a mixture of different tags [8]. Here, we present R_b results obtained from three variations of $b\bar{b}$ event tagging methods used by the TASSO [10] and Mark II [11] experiments. The b-tag cuts are applied to either the number of tracks with large impact parameters or the number of reconstructed vertices inconsistent with the primary vertex. These tags do not have to be corrected for the b semileptonic branching ratio which is needed for the lepton tags. They do not depend strongly on the simulation of the event sphericity as the event shape b tags are. Last, they do not depend on modeling of the correlation between the hemispheres of the event as do the hemisphere b tags.

The SLAC Large Detector (SLD) with its precision vertex detector has excellent resolution for measuring decay lengths and separating secondary vertices from primary vertices. The SLAC Linear Collider (SLC) e^+e^- beams collide at the SLD interaction point with center of mass energy equal to the Z^0 peak. The small and stable Z^0 production point provided by the SLC combined with the precision of the detector enhances the use of methods which directly exploit the B hadron lifetime to tag $b\bar{b}$ events with high efficiency and low contamination.

The content of this paper is organized as follows. The SLD and the performance of its components used in this analysis are introduced. The means of determining the event production point is presented. The Monte Carlo (MC) simulation used in determining the tagging efficiencies is outlined. The details of the event and track selection are then described. Finally, R_b results along with systematics and verification checks are given.

II. SLAC LARGE DETECTOR

During the 1992 and 1993 runs over 60k Z^0 events produced by the SLC were recorded by the SLD. A subset of these events constitutes the fiducial sample for the analyses presented here. Details of all SLD components are described elsewhere [9]. Here we describe only the de-

tector elements used for this analysis, namely, the vertex detector (VXD), the central drift chamber (CDC), and the liquid argon calorimeter (LAC) operating in a 0.6 T magnetic field.

A. Vertex detector

The close proximity of the VXD [12] to the beam line and the precise three-dimensional (3D) hit locations it provides allow a clear distinction of secondary vertices from the primary vertex. The VXD consists of 480 charge coupled devices (CCD's) as the basic detector elements. Each CCD consists of 20 μm thick active epitaxial silicon residing on a 180 μm p^+ silicon substrate and contains 375×578 22 μm square pixels. Eight CCD's mounted on an alumina mother board with printed electrical connections comprise a ladder. Each ladder has 4 CCD's on the top face and 4 on the bottom face, spaced so as to leave no gaps in the CCD coverage along the length of the ladder. There are 60 ladders arranged in 4 concentric layers with each ladder having an active length of 92 mm. The innermost ladders are located 29 mm from the beam line and the outermost ones at 41 mm. The geometry of the VXD is shown in a cross section transverse to the beam line in Fig. 1. The innermost (outermost) layer subtends a range of $|\cos\theta| < 0.85$ (< 0.75). The spacing of the ladders in ϕ is such that there are no gaps in the ϕ coverage of the CCD's between the first and last pairs of layers. A track coming from the interaction point is guaranteed to pass through two CCD's, with the average being 2.3. Dark current in the detector is reduced to a negligible level by operating at a temperature of 195 K using cold nitrogen gas flowing throughout the VXD. A low mass cryostat surrounding the VXD insulates it from the rest of the detector. The ladder support system is made of beryllium to reduce multiple scattering and provide maximal mechanical stability. A 1 mm thick beryllium beam pipe with a 100 μm Ti liner is located at a radius of 25 mm. Including a 0.5 mm beryllium gas shell, the total material before the first CCD layer is 0.71% radiation length (r.l.); for each CCD layer traversed at normal incidence a particle will see ~1.1% r.l. (See Table I.) Approximately 4% of the CCD channels were found to be faulty immediately after installation mostly due to inaccessible connection problems. No further degradation in the performance of the CCD's, their connections, or the front end electronics was observed during the 1992 or 1993 runs.

B. Central drift chamber

Charged track momentum measurements are made using the CDC [13] which is 1.8 m long and extends radially from 0.2 m to 1.0 m. It consists of ten superlayers, four coaxial to the beam with each of these separated from the next by two with stereo angles of ±41 mrad. Each superlayer consists of cells 50 mm along the radius and ~ 59 mm wide in azimuth at the midpoint. Each of the 640 cells contains eight 25 μm diameter gold-plated tungsten sense wires separated radially by 5 mm. Eighteen 150 μm diameter gold-plated aluminum field shaping wires are placed 3.5 mm from either side of the sense wire plane. Two additional field shaping wires at the top and bottom of the cell plus twenty-five 150 μm diameter gold-plated aluminum field wires surrounding the cell complete the field shaping. The geometry of the CDC as seen from one end of the detector is shown in Fig. 2.

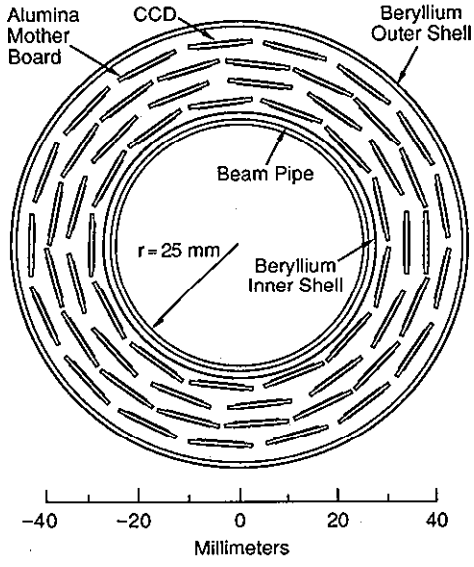

FIG. 1. xy cross section of the VXD geometry. There are 60 ladders with 4 CCD's on the top face and 4 CCD's on the bottom face of each ladder.

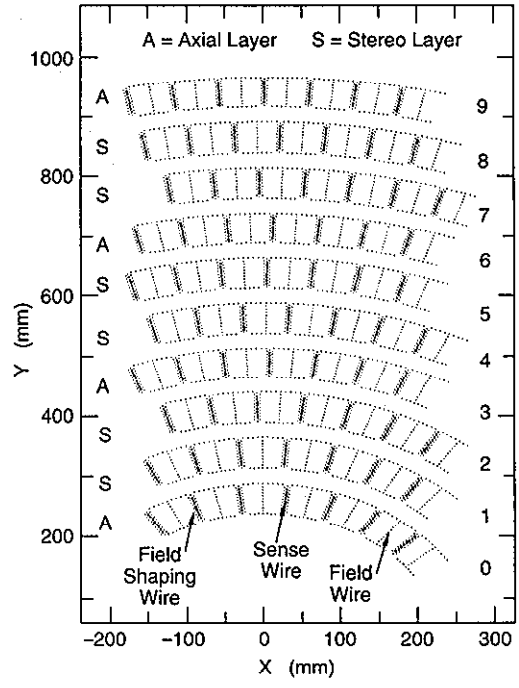

FIG. 2. xy cross section of a portion of the CDC end plate showing the relative location of sense and field wires.

TABLE I. Radiation lengths seen by a track passing through the central tracking volume at $\theta = 90°$. It should be noted that on average a track will only pass through 2.3 ladders.

	Mean radius (mm)	L/L_R (%)
Ti liner	25.0	0.28
Be beam pipe	25.5	0.28
Be inner shell	27.0	0.14
Layer 1 ladder	29.5	1.15
Layer 2 ladder	33.5	1.15
Layer 3 ladder	37.5	1.15
Layer 4 ladder	41.5	1.15
Be outer shell	45.5	0.20
N_2 gas	80.0	0.06
Cryostat	165.5	0.98
CDC inner wall	200.0	1.80
CDC gas	600.0	0.50
CDC wires	600.0	0.20

The sense and field shaping wires of a cell are strung as a unit to a Lexan block so that the relative positions of the wires within a cell are fixed and well known. Readout for pulse heights and times of hits is implemented on both ends of the wires. This information is used to derive the drift times and charge division of the hits. An average spatial resolution of 70 μm is obtained with a cool gas of CO_2:argon:isobutane in the ratio of 75% : 21% : 4%, respectively. The chamber is operated at atmospheric pressure. The radiation lengths of material seen by a track passing through the central tracking volume are listed in Table I.

C. Liquid argon calorimeter

The LAC [14] is used in the hadronic event trigger and in determining the thrust axis direction for event acceptance cuts. The LAC barrel inner radius is 1.77 m and extends to 2.91 m. The barrel and end caps consist of lead plates separated by liquid argon. The barrel covers $|\cos\theta| < 0.84$ and end caps cover $0.82 < |\cos\theta| < 0.98$ for the full azimuthal range. Each has a 21 radiation length thick electromagnetic (EM) section before a 2.0 absorption length hadronic (HAD) section. In the barrel the azimuthal segmentation ($\Delta\phi$) for the EM section is 33 mrad and the polar segmentation($\Delta\theta$) is given by $\frac{\Delta\theta}{\sin\theta}$=36 mrad. In both the polar and azimuthal dimensions the HAD towers are twice the size of the EM towers. The projective area of the towers in the end caps is approximately the same as the barrel. The energy resolution of the calorimeter barrel for electromagnetic showers of energy E is measured to be $\frac{\sigma}{E} = \frac{15\%}{\sqrt{E(\mathrm{GeV})}}$ and $\frac{60\%}{\sqrt{E(\mathrm{GeV})}}$ for hadronic showers.

III. TRACKING PERFORMANCE

The analyses in this paper rely critically on the performance of the tracking systems. The first stage of track reconstruction is done in the CDC with pattern recognition followed by track fitting. The second stage leading to a combined CDC and VXD track is then performed by extrapolating the CDC track into the VXD and linking to the best set of VXD hit pixel clusters. A combined track fit is performed using the Billoir [15] method to take into account the track multiple scattering through detector material.

The CDC track pattern recognition is aided by the charge division with a resolution of $\sim$ 6 cm along the wire, while the final track fit only uses the drift time information from axial and stereo wires. The cell-by-cell wire block position alignment is determined from tracks [16] with constraints provided by the known mechanical construction tolerances. Isolated tracks in hadronic Z^0 decay events are used to determine the local cell offsets and tilts, while $Z^0 \to \mu^+\mu^-$ and cosmic ray events are used to remove long range global misalignment features. The CDC spatial resolution achieved is 50–100 μm for most parts of a cell and $\sim$200 μm near the sense and field wires. The azimuthal angle and polar angle resolution on the track direction at the inner radius of the CDC are 0.45 mrad and 3.7 mrad, respectively, for high momentum tracks.

The VXD hit cluster linking includes a final pass to allow linking to just one VXD hit with a loose beam constraint during pattern recognition. This results in a uniform track VXD linking efficiency around the full azimuth without degradation for regions with malfunctioning ladders. Each VXD hit cluster is only allowed to be associated with one track. This mainly removes tracks produced in particle interactions with detector material which linked to wrong VXD hits. Correctly linked tracks very rarely lose hits in this arbitration process due to the fine granularity of the 3D pixels. For all good CDC tracks within the VXD acceptance, with transverse momentum $P_\perp > 300$ MeV/c and which extrapolate to the proximity of the interaction point, 93% link to VXD hits in the data. This agrees with the MC simulation to within 1%. Of these CDC tracks there are still tracks resulting from long-lived particle decays and products of interactions with detector material which should not have VXD links. MC studies indicate that for CDC tracks from primary vertex and heavy hadron decays, 96.2% are correctly linked with VXD hits. Of the remaining tracks 2.3% have no VXD link and 1.5% linked with at least one wrong VXD hit.

The VXD ladders and barrel structures were optically surveyed before installation [12,17]. The individual ladder survey provides relative locations of CCD's on the same ladder while the barrel structure survey supplies the ladder locations for an initial VXD geometry. The VXD internal ladder-to-ladder alignment is then performed using tracks in Z^0 decay events, allowing each ladder to shift, rotate, and bow while relative locations of CCD's on each ladder are fixed according to optical survey measurements. The tracks in all Z^0 decay events which have hits in three or more VXD layers are used to provide local constraints between layers, while the $Z^0 \to \mu^+\mu^-$ and $Z^0 \to e^+e^-$ events are used to provide global constraints. Special attention is paid to the matching of

CDC tracks and VXD hit vectors globally and as a function of ϕ in both the CDC and VXD alignment procedures. The VXD internal alignment parameters show very good consistency between 1992 and 1993 data, indicating that the beryllium support structure has indeed ensured the integrity and stability of the VXD internal geometry over a long period of time against thermal cycling. As a last step of the alignment procedure, the VXD is treated as a rigid body and its rotation and shift with respect to the CDC are determined using tracks in hadronic Z^0 events. The overall VXD spatial resolutions achieved, including intrinsic and remaining alignment errors, are estimated from tracks with hits in three layers (see Fig. 3) and from the miss distance for $Z^0 \to \mu^+\mu^-$ and $Z^0 \to e^+e^-$ tracks fitted to VXD hits alone with a momentum constraint. The two methods obtained very similar results corresponding to a single hit $r\phi$ resolution of 5.5 μm over all $\cos\theta$ and effective z resolution of 5.5 μm at $\cos\theta = 0$ and 9 μm averaging over tracks at $|\cos\theta| > 0.55$. The deterioration of effective z resolution at high $|\cos\theta|$ is primarily due to alignment errors in the ladder radial position and shape.

The impact parameter resolution obtained from combining the CDC and VXD hits for high momentum tracks is determined from the two-track miss distance using $Z^0 \to \mu^+\mu^-$ events. The single-track impact parameter resolution is found to be 11 μm in the $r\phi$ view and 38 μm in the rz view. The significantly better resolution in the $r\phi$ view is due to the much more accurate CDC track ϕ angle resolution compared to polar angle resolution used in the combined fit. The impact parameter resolution for lower momentum tracks is determined from hadronic Z^0 data and using the MC simulation to correct for contributions from heavy hadron decay and uncertainty in the interaction point position. The impact parameter resolution obtained for 1 GeV tracks at $\cos\theta = 0$ is 76 μm in the $r\phi$ view and 80 μm in the rz view. The momentum resolution for the combined CDC and VXD track fit is $\frac{\delta p_\perp}{p_\perp} = 0.01 \oplus 0.0026 p_\perp$. The combined track fit also improves the track momentum direction resolution near the interaction point by 30% in ϕ and 40% in θ compared to the CDC-alone track.

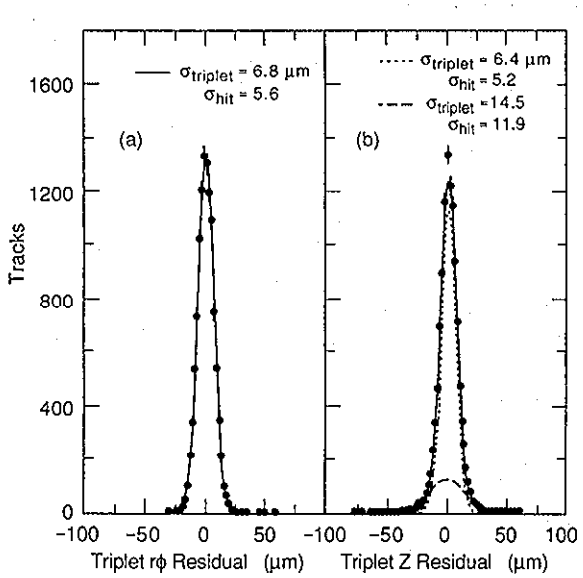

FIG. 3. Plot of the residual of the middle hit in a triplet of VXD hits from the same track on three separate layers relative to track which is forced to go through the first and last hit of the triplet. All tracks with momentum greater than 1 GeV/c for all $\cos\theta$ in hadronic Z^0 events are used. The single-hit resolution ($\sigma_{\rm hit}$) is obtained from the triplet miss distance by dividing by 1.22 to account for broadening due to the finite resolution of the other two hits at an average lever arm ratio.

IV. PRIMARY VERTEX DETERMINATION

An accurate knowledge of the individual event primary vertex (PV) position is necessary as a reference location to distinguish secondary vertices in $b\bar{b}$ events. The best estimate of the PV in the transverse plane is the average SLC interaction point[1] ($\langle$IP$\rangle$). The size of the SLC luminous region is much smaller in the transverse dimensions ($\sigma \sim$ 2–3 μm in x and 0.5–1 μm in y) than in the beam direction ($\sigma_z \sim 700\,\mu$m). For this reason, the $\langle$IP$\rangle$ $r\phi$ position is determined with track parameters and errors from many sequential hadronic events. Because of the large spread of the luminous region in the beam direction, the longitudinal position of the PV is determined for each event individually.

A. Transverse position

If tracks consistent with coming from the Z^0 PV in a single hadronic event are fit to a common vertex in the $r\phi$ plane, the PV fit error ellipse is typically $\sim 100\,\mu$m along the major axis and $\sim 15\,\mu$m transverse to the minor axis. This $\sim 15\,\mu$m would be the PV contribution to the impact parameter error of a track in the direction of the major axis, which is approximately the direction of the thrust axis. Tracks at large angles to the thrust axis have significantly larger errors.

The motion of the SLC IP for the time period over which events are averaged is estimated to be $\sim 6\,\mu$m determined by monitoring the corrector magnets which keep the SLC beams in collision. This means that the $\langle$IP$\rangle$ $r\phi$ position is a better estimate of the PV position in an event than the one found with tracks from only that event. Using the $\langle$IP$\rangle$ as the PV position substantially reduces the uncertainty in the PV location due to single-track resolution, and removes the elongation of the PV error ellipse in the direction of the thrust axis, as the ϕ distribution of thrust axes is isotropic. In addition, by averaging over many events to determine the IP position, systematic errors due to the difficulty of finding the correct PV in events with many secondary decay vertices

[1]The IP position is the center of the luminous interaction region within which the PV is located.

are greatly reduced.

An ⟨IP⟩ is determined for each set of 20–30 sequentially recorded Z^0's. All tracks which have VXD hits and which come within 3σ of a trial ⟨IP⟩ are fit to a common vertex. Typically 330 tracks are used in a fit. The fit ⟨IP⟩ is then used as a new trial ⟨IP⟩, and the process is iterated until it converges. The $\chi^2/N_{\rm DF}$ and the fraction of tracks within 3σ of the fit ⟨IP⟩ are checked for each set, along with the time history of the x and y ⟨IP⟩ positions, to identify sets which might span a major shift in IP position. The $\chi^2/N_{\rm DF}$ is required to be < 1.3, and the number of tracks used in the fit is required to be more than 8 times the number of events in the set. Information from the SLC correctors is used to help determine exactly when a major shift occurs. When a major shift is found within a set, the boundaries of the set are changed to coincide with where the IP shift occurs while still maintaining ~ 30 events per set whenever possible, and the fitting procedure is repeated.

The fit ⟨IP⟩ position for the set in which an event resides is then used as the best estimate of the PV $r\phi$ position for that event. Typically any one event contributes only a few percent of the tracks used in the fit. The uncertainty in the ⟨IP⟩ ($\sigma_{\rm IP}$) is the convolution of the statistical error from the fit ($\sim 3\,\mu$m), the extent of the SLC luminous region ($\sim 1\,\mu$m), and the motion of the IP within a set ($\sim 6\,\mu$m), giving a total of $\sim 7\,\mu$m when added in quadrature. Several methods are used to estimate $\sigma_{\rm IP}$ from the data. The distribution of track impact parameters with respect to ⟨IP⟩ in $\mu^+\mu^-$ events (shown in Fig. 4 for the 1993 data) is a good independent measure, as $\mu^+\mu^-$ and e^+e^- events are not used in any way for the determination of ⟨IP⟩. The σ of the distribution is 12.7 μm; when the track extrapolation error, measured from $\mu^+\mu^-$ miss distance, is subtracted in quadrature, this gives $\sigma_{\rm IP} = 6.7\,\mu$m. In hadronic events where most tracks fit to a common vertex, the distance (y_T) between the ⟨IP⟩ and the fit vertex, projected onto the minor axis of the fit vertex error ellipse, also contains information on $\sigma_{\rm IP}$. This y_T distribution, while having high statistics, includes some contamination from $Z^0 \to b\bar{b}$ and $c\bar{c}$ events. A second sample where all tracks fit to a common vertex is a very pure sample of light quark events but is significantly lower in statistics. The y_T distributions for both these samples were studied, along with the $\mu^+\mu^-$ and e^+e^- track impact parameter distributions, and all distributions agree with $\sigma_{\rm IP} = 7\,\mu$m$\pm 2\,\mu$m ($9\,\mu$m$\pm 2\,\mu$m) for the 1993 (1992) data.

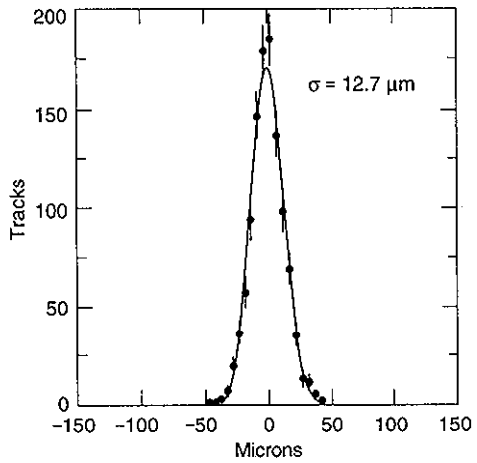

FIG. 4. Distribution of track impact parameters in $\mu^+\mu^-$ events with respect to the ⟨IP⟩ determined from hadronic events.

Even though the procedure for finding the ⟨IP⟩ is set up to minimize large beam motion in each set, it is still possible that a few sets contain events which occur far from the ⟨IP⟩. The same distributions which are used to estimate $\sigma_{\rm IP}$ are searched for evidence of non-Gaussian tails. The cleanest of the checks, the $\mu^+\mu^-$ impact parameter distribution, shows no evidence for non-Gaussian tails, but because $\Gamma_{Z^0\to\mu^+\mu^-} \ll \Gamma_{Z^0\to\rm hadrons}$, this in itself cannot conclusively rule out non-Gaussian tails on ⟨IP⟩. The highest statistics check, the y_T distribution in hadronic events where most tracks fit to a common vertex, shows that the MC simulation and data have similar non-Gaussian tails. The MC simulation indicates that this tail is due to the occasional inclusion of B or D decay tracks in the vertex fit. All other distributions show smaller non-Gaussian tails than this one. The non-Gaussian tails in all the distributions are conservatively represented by a second IP spread ($\sigma'_{\rm IP}$) of 100 μm in $< 0.25\%$ ($< 0.5\%$) of the events collected in 1993 (1992).

B. Longitudinal position

The best estimate of the PV z position for an event comes from a technique using only the median z of tracks in the event itself. Each track with associated VXD hits is extrapolated to the point of closest approach (POCA) to the ⟨IP⟩ in the $r\phi$ view and the z coordinate of the track at this point is denoted as $z_{\rm POCA}$. A selection of tracks is then made to require the track $r\phi$ impact parameter to the ⟨IP⟩ to be less than 500 μm and consistent with originating from the $r\phi$ ⟨IP⟩ within 3σ based on the estimated track impact parameter error and ⟨IP⟩ error. The event IP z location is simply defined as the *median* of the $z_{\rm POCA}$ values from the selected tracks. For the small fraction of events with no tracks passing this selection, all tracks with VXD hits are used. The choice of the median z method instead of the more common approach involving vertexing is based on the result of a MC study, showing that the median z is more robust against the effect of inclusion of tracks not originating from the PV. The typical resolutions of locating the PV z as derived from MC simulation using rms of the residual $z_{\rm estimate} - z_{\rm true}$ are (32,36,52) μm for (uds, c, b) events, respectively. The tails of the PV z residual distributions can be characterized by the fractions of events with residual $> 100\,\mu$m. The fractions of such events are (0.8%,1.6%,7.5%) for (uds, c, b) events, respectively, according to the MC simulation.

V. MONTE CARLO SIMULATION

The analyses use the flavor tagging efficiencies, estimated from the MC simulation, to determine R_b from

the rate at which events are tagged in the data. It is therefore necessary to have an accurate simulation of Z^0 event properties and detector response.

A. Monte Carlo physics modelling

The $Z^0 \to$ hadrons MC events are simulated using the JETSET 6.3 [18] generator framework. The QCD parton shower and LUND string fragmentation parameters used are the same as those determined by TASSO at $\sqrt{s}$ =35 GeV [19], and have been found to be in good agreement with data at the Z^0 energy [20]. The heavy flavor fragmentation functions used for the b and c quarks are according to Peterson *et al.* [21] with ϵ_b=0.006, and ϵ_c=0.06, respectively. The resulting average energy of $\langle x_E \rangle$=0.695 for B hadrons in $b\bar{b}$ events and $\langle x_E \rangle$=0.501 for D^* mesons in $c\bar{c}$ events is in good agreement with the existing measurements [22]. The mean event total charged particle multiplicity of $\langle n_{\rm ch} \rangle$=21.1 from this MC simulation is also consistent with the experimental measurements [23].

The production rates for D^0, D^+, D_s mesons and Λ_c baryons are 59.0%, 19.5%, 12.6%, and 8.9%, respectively. The decays of D^0, D^+, D_s mesons and Λ_c baryons are simulated with exclusively tabulated branching ratios based on measurement results listed in the Particle Data Group review [24]. Some unmeasured decay modes are also included with branching ratios according to expectations from isospin symmetry in comparison with measured decay modes. Decay modes with large measurement errors are adjusted within tolerance to reproduce the observed inclusive production rates of leptons, kaons, [24] and the D meson decay charged multiplicity distributions from Mark III [25]. The charm meson three-body semileptonic decay simulation uses the Wirbel-Stech-Bauer (WSB) [26] form factor model, while all remaining decay modes are simulated by phase space distribution. The decays of weakly decaying charm baryons other than Λ_c are simulated using the JETSET 6.3 [18] heavy flavor decay package. The D^{*+} and D^{*0} decay branching ratios in the MC simulation are updated to the recent measurements from CLEO [27].

B hadron decays are simulated via a hybrid heavy hadron decay model. The B baryon decay simulation uses the unmodified LUND 6.3 heavy hadron decay package [18], while the B meson decay simulation involves several parts as follows.

A total of 25.0% of the simulated B meson decays are semileptonic. The Isgur-Scora-Grinstein-Wise (ISGW) [28] form factor model is used with the inclusion of D^{**} production. The fractions of decays producing charmed spectator mesons D, D^*, and D^{**} is chosen to be 0.33, 0.58, and 0.09, respectively, in our MC simulation. The semileptonic branching fractions to electrons, μ's, and τ's are set to 11.0%, 11.0%, and 3.0%, respectively. The resulting MC lepton momentum spectrum from B_u, B_d decays in the B rest frame, including the leptons from $b \to c \to \ell$, is in reasonable agreement with the recent CLEO data [29].

A total of 12.5% of the branching fraction for each B meson is simulated with exclusively tabulated branching ratios based on various observed two body hadronic decays [24].

A total of 6% of the B meson branching fractions in the MC simulation are produced containing charm baryons in the decay. Baryon production in B meson decay simulation is controlled explicitly to only occur in association with charm baryon production based on the conclusion from CLEO [30]. The charm baryons are produced by means of internal W-emission diagrams with diquark popping in the fragmentation involving the charm quark.

The remaining 56.5% of the branching fraction is simulated via the LUND 6.3 heavy hadron decay package [18], extensively tuned so that the average B_u, B_d decays in the full model provide a good representation of inclusive particle production for B meson decays measured at the $\Upsilon(4s)$. In this model, the weak decay matrix element is used to specify the four momenta of the quark-level decay products of b quark decay. Two separate $q\bar{q}'$ systems are formed from the b quark decay product and the spectator antiquark. The system involving the spectator is then collapsed into a single particle, while the other system is allowed to fragment according the standard LUND scheme for particle branching and flavor assignment with fragmentation product distributed kinematically according to a phase-space distribution. The fractions of D^{**} production and internal W emission are tuned to provide a good description of the charm hadron momentum spectrum in B meson decays as measured by CLEO [31]. Adjustments are also made to the vector or pseudoscalar particle production ratios and strange quark yield in the fragmentation to achieve a good description of various measured particle production fractions and momentum spectra.

The resulting MC inclusive production rates for various particles averaged between B_u and B_d meson decays are listed in Table II together with the current measurement

TABLE II. MC average B_u, B_d meson decay inclusive particle yield compared to experimental measurements.

Decay type	MC $\langle B_u, B_d \rangle$	Measurements			
$B \to e$	0.110	0.104	$\pm$	0.004	[36]
$B \to \mu$	0.110	0.103	$\pm$	0.005	[36]
$B \to \tau$	0.030	0.041	$\pm$	0.010	[36]
$B \to D^0$	0.629	0.621	$\pm$	0.026	[32]
$B \to D^+$	0.259	0.239	$\pm$	0.037	[32]
$B \to D_s$	0.099	0.100	$\pm$	0.025	[32]
$B \to D^{*+}$	0.236	0.230	$\pm$	0.040	[36]
$B \to$ charmed baryons	0.060	0.064	$\pm$	0.011	[36]
$B \to J/\psi$	0.014	0.013	$\pm$	0.002	[36]
$B \to D^{(*)} D_s^{(*)}$	0.065	0.050	$\pm$	0.009	[36]
$B \to \pi^\pm$ (direct)	3.564	3.59	$\pm$	0.11	[35]
$B \to K^\pm$	0.765	0.78	$\pm$	0.04	[35]
$B \to K^0$	0.692	0.64	$\pm$	0.04	[35]
$B \to$proton	0.092	0.080	$\pm$	0.005	[36]
$B \to \Lambda$	0.023	0.040	$\pm$	0.005	[36]
$B \to$ charged tracks $\times$ 2	10.95	10.81	$\pm$	0.24	[33]
		10.99	$\pm$	0.30	[34]

values for comparison. Besides the lepton and charm meson momentum spectra in the B decay rest frame, the momentum spectra of $\pi^{\pm}, K^{\pm}, K^0$ and protons for average B_u, B_d decays in the MC are also checked and found to be in good agreement with the ARGUS measurements [35]. The charged track multiplicity for average $B_u\overline{B_u}$ and $B_d\overline{B_d}$ decays also gives a good description of the measured $\Upsilon(4s)$ decay charged multiplicity distribution [33,34].

All mean decay lifetimes of charm hadrons used in the MC simulation are from the 1992 Particle Data Group review [24]. The mean decay lifetime of B hadrons in the MC simulation are set to 1.55 ps for B mesons and 1.10 ps for B baryons, which are in good agreement with current measurements [36]. The B baryon production in the MC simulation amounts to 8.9% of B hadron production which in turn translates to an average MC-simulated B hadron lifetime of 1.51 ps.

B. Detector simulation

The MC detector simulation is based on GEANT 3.15 [37], with a detailed geometric description of the SLD, and produces data that models the detector's response to charged and neutral particles. Simulated Z^0 events are overlaid with signals from events taken on random beam crossings in close time proximity to each recorded real Z^0 and then processed using standard reconstruction as for data. Information about dead detector channels and the high voltage status of CDC layers from the random beam crossing events are used to simulate detector performance. These random beam crossing events also assist in simulating precisely the geometric and time-dependent pattern of beam backgrounds, detector readout noise, and trigger conditions. The detector geometry is smeared to reflect uncertainties remaining after the detector alignments have been performed. The simulation elements mentioned here result in a MC program with a properly luminosity weighted overall detector response and machine background with the same time dependence as in the data.

VI. EVENT AND TRACK SELECTION

A. Event trigger

The event trigger requires at least 15 GeV of energy in LAC towers passing a high threshold cut (240 MeV for EM towers, 1.2 GeV for HAD towers). At least ten towers must have contributed to the energy sums with at least one being in the forward and one being in the backward sections of the barrel. Additionally, a track must have been found in the CDC. A track is identified, in the acquisition system, by constructing a map of cells which have hits on at least four wires. Then the list of these cells versus superlayer is compared against a lookup table for combinations which are consistent with nearly straight tracks. Any matching combination indicates a track. To avoid triggering on beam background bursts the trigger is vetoed if the number of CDC cells with at least six of the eight wires hit is > 275.

B. Event selection

Events passing the trigger are required to have at least 18 GeV of energy as measured from charged tracks. The thrust axis, determined from calorimeter clusters, is required to be in $|\cos\theta| < 0.71$ which is well within the VXD acceptance. At least seven CDC tracks are required to be present to assist in eliminating $\gamma\gamma$ and $\tau^+\tau^-$ events. At least one CDC track must have hits from the first or second CDC layer to ensure that the high voltage to these layers is on. At least three tracks with two or more VXD hits must be found. A fiducial set of 16K (5K) Z^0 events is obtained from 1993 (1992) data. The corresponding sample of MC events is 84K (22K) for 1993 (1992). The nonhadronic background (primarily $\tau^+\tau^-$) is $< 0.2\%$, as determined from the MC program. The flavor bias potentially introduced by trigger and event selection for b quarks relative to light flavor Z^0 events is determined from the MC program. No bias was observed within Monte Carlo statistical errors.

C. Track selection

Poorly measured tracks and tracks resulting both from interactions with the detector material and from long-lived particle decays often have large impact parameters that can lead to contamination of the b-tagging signal. These tracks can be efficiently removed by requirements on the measured production point of the tracks and by identifying and removing long-lived neutral particles that decay into a pair of tracks (V^0) before leaving the track detection region.

Well-measured tracks are selected by requiring that the CDC track start at radius < 39.0 cm and have > 40 hits. The CDC track is required to extrapolate to within 1 cm of the $\langle$IP$\rangle$ in xy, and within 1.5 cm of the PV in z to eliminate tracks from interaction with the detector material and poorly measured tracks. The fit of the CDC track must also satisfy $\chi^2/N_{\rm DF} < 5$. At least one VXD hit is required, and the combined CDC/VXD fit must satisfy $\chi^2/N_{\rm DF} < 5$. Tracks with xy impact parameter errors $> 250\ \mu$m or with xy impact parameters > 3.0 mm with respect to the $\langle$IP$\rangle$ are removed. The impact parameter error cut acts both as a quality cut and an effective minimum momentum cut. Tracks passing all criteria mentioned above will be referred to as quality tracks.

V^0's from K^0_S decays and Λ decays are identified by searching for pairs of charged tracks forming a neutral vertex significantly displaced from the $\langle$IP$\rangle$ with a mass consistent with a K^0_S or Λ. γ conversions are identified by searching for track pairs of opposite charge which, when the tracks are assigned the mass of an electron, are consistent with a near-zero parent mass at the point where the tracks are parallel to each other in the $r\phi$ view.

Loose requirements on the separation of the tracks at the vertex position and the opening angle of the tracks are applied. Any track found to belong to a V^0 is eliminated.

1. Tracking efficiency corrections

The fraction of tracks passing the quality cuts is different between the data and MC simulation. This is primarily due to a simplified simulation of the dependence of the CDC hit efficiency and resolution on the position within a CDC cell. The hit efficiency and resolution near the field wires are too optimistic in the MC simulation. The MC simulation is corrected to yield the proper fraction of quality tracks by systematically removing tracks according to the discrepancy between the data and MC simulation on the fraction of CDC tracks classified as good and on the CDC-to-VXD linking rate for the good CDC tracks. The correction is performed by determining the difference between the data and MC simulation on the quality track multiplicity fraction in the ranges of $p_\perp$, $\cos\theta$, ϕ, and the angle with respect to the jet direction for CDC tracks and in the difference in fraction of good CDC tracks that link to VXD hits in the ranges of p, $\cos\theta$, and ϕ. About 6% of the MC tracks are removed to correct for both the good CDC and linking fractions. The dependence of the corrections on the various variables is found to be small which reflects the random nature of the CDC track misreconstruction despite the correlated local hit loss within a cell. This is an expected result of the geometry having a large number of staggered small cells.

2. Tracking resolution corrections

The distribution of track impact parameters after suppression of the track population from long-lived particle decays is used to check the MC impact parameter resolution. This distribution is generated by using only tracks that appear to originate behind the primary vertex with respect to the jet axis with which the track is associated. Details of the method are given in Sec. VII A 1. These lifetime-depleted impact parameter distributions from the data and MC simulation are compared in the $r\phi$ and rz projections for different $p_\perp$ and $\cos\theta$ regions to examine the quality of the MC simulation for impact parameter resolution. The non-Gaussian tail of the impact parameter distribution in the data is found to be well described by the MC simulation in both $r\phi$ and rz projections. The core of the MC $r\phi$ impact parameter distribution is observed to be broader than the data by ~8%. This is caused by a slightly pessimistic alignment error used for the VXD CCD position smear in the MC simulation. Corrections for this effect are applied to the reconstructed MC track $r\phi$ impact parameters using the MC information of the true origin of the tracks. The core of the MC rz impact parameter distribution on the other hand is observed to be narrower than the data. This is the result of some remaining systematic misalignment effects mainly in the VXD ladder bowing shape and the ϕ-dependent CDC and VXD track polar angle matchings, which have little effect in the VXD spatial resolution estimate but become more significant for the combined CDC and VXD track fit. The MC track z coordinates at the xy point of closest approach ($z_{\rm POCA}$) are adjusted to mimic the effects in the data. A Gaussian smear of $\frac{16}{\sin\theta}$ μm is applied to the MC track $z_{\rm POCA}$ in addition to a systematic ϕ-dependent shift of $z_{\rm POCA}$ with magnitude typically around $\pm 20\,\mu$m. The corrections mentioned here are used in the analyses but the distributions of Fig. 5 referred to in Secs. VII A, VII B, and VII C are shown without tracking resolution corrections.

VII. R_b MEASUREMENTS

R_b is measured by isolating $b\bar{b}$ events using tags on the lifetime information from the quality tracks in the fiducial sets of events from the MC simulation and data. For each b tag the rate at which events are tagged in data and the efficiencies for tagging each flavor ($b\bar{b}$, $c\bar{c}$, and $u\bar{u}+d\bar{d}+s\bar{s}$), estimated from the MC simulation, are used to calculate R_b:

$$R_b = \frac{f_{\rm tag} - \epsilon_{uds} - (\epsilon_c - \epsilon_{uds})R_c}{\epsilon_b - \epsilon_{uds}}, \qquad (1)$$

where $\epsilon_i = N^i_{\rm tagged}/N^i_{\rm input}$ $i = (b,\, c \text{ or } uds)$ from the MC simulation and $f_{\rm tag} = N^{\rm data}_{\rm tagged}/N^{\rm data}_{\rm input}$ from the data. The denominators $N^i_{\rm input}$ and $N^{\rm data}_{\rm input}$ are the number of data and MC events which passed the selection cuts. The standard model value for the c fraction, $R_c = \frac{\Gamma(Z^0\to c\bar{c})}{\Gamma(Z^0\to {\rm hadrons})} = 0.171$, is used for determining R_b. The purity of the b-tagged sample, Π_b, is used as a monitor of the quality of the b tag. It is defined as the fraction of $b\bar{b}$ events in the tagged MC sample using standard model values for R_b and R_c. The MC simulation generates an R_b of 0.215.

Three tag methods have been used which take advantage of different abilities of the tracking systems to obtain a high ϵ_b while minimizing systematics resulting from modeling of light quarks by having a high purity for the b-tagged sample. The mechanics of the tags and the results obtained are given below.

A. 2D impact parameter tag method

The 2D impact parameter method utilizes the excellent $r\phi$ resolution of the tracking systems, the accurate ⟨IP⟩ knowledge in the $r\phi$ plane and the simplified detector resolution systematics in this plane.

1. Impact parameter signing

The track 2D impact parameters are signed to indicate whether the track originates in front or behind the PV with respect to the jet axis. The JADE jet finding algorithm [38] with $y_{\rm cut} = 0.02$ is used on tracks in the event

to determine the jet axes and to obtain the track-to-jet associations. The $y_{\rm cut}$ is chosen to minimize misassignments of tracks to jets while maintaining an accurate estimate of the b-hadron flight direction. An average of 2.6 jets per Z^0 event is found. Each track is assigned a positive (negative) impact if it crosses its jet axis in front (back) of the $\langle$IP$\rangle$. This is determined from the sign of the 2D dot product of a vector from the $\langle$IP$\rangle$ to the tracks xy point of closest approach to the $\langle$IP$\rangle$ with the jet axis direction. Secondary decay tracks preferentially populate positive impact parameters due to the lifetime of the parent particle. Negative impact parameter tracks are most often the result of tracking resolution, poorly measured tracks, products of interactions in the detector material, and IP position resolution. Some lifetime information does appear in the negative impact parameter distribution, as negative impact parameters can naturally occur for tertiary decays and as a result of errors in jet assignment and direction.

The significance of the track impact parameter is used as the tagging variable for the tracks. The significance is given by the signed and normalized impact parameter $\delta_{\rm norm} = \frac{\delta}{\sigma_\delta}$, which is formed from the signed impact parameter divided by the error on the track extrapolation combined with the beam position error. The negative normalized impact parameter distribution is used to test the MC resolution simulation by comparing the MC simulation and data. The $\delta_{\rm norm}$ distribution of the data and MC simulation are shown in Fig. 5.

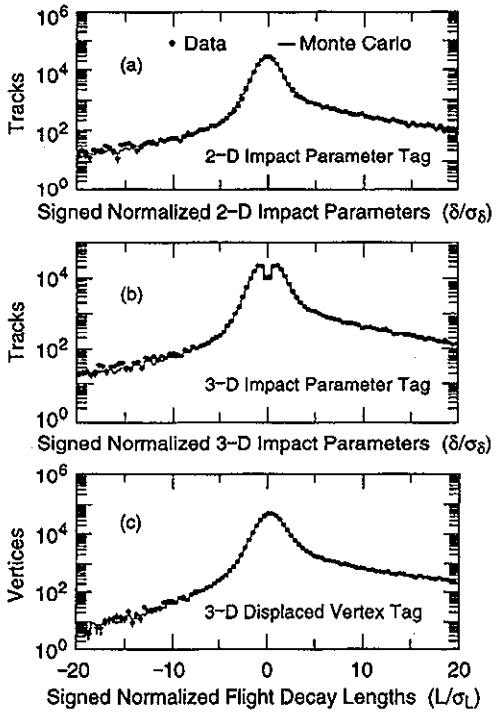

FIG. 5. Data and Monte Carlo signed normalized 2D and 3D impact distributions, and signed normalized flight decay length distributions without tracking resolution corrections for the MC simulation.

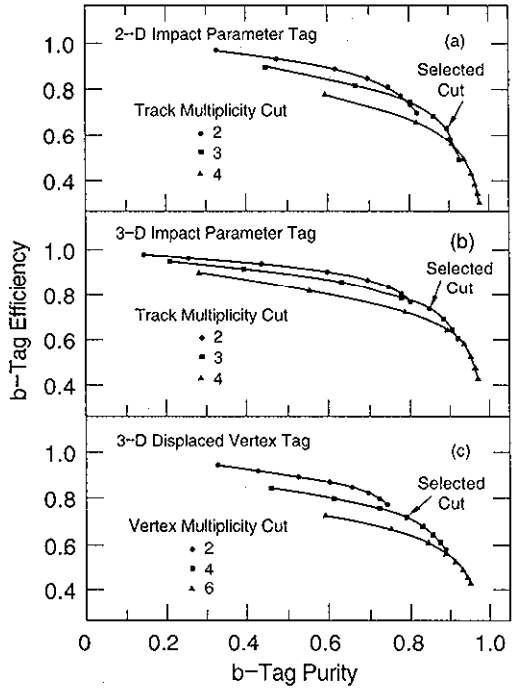

FIG. 6. $b\bar{b}$ event tagging efficiencies versus purities for each $b\bar{b}$ event tagging method with different multiplicity and significance cuts, derived from the Monte Carlo simulation. Each curve represents the estimated efficiencies and purities as the significance cut is varied from 1.5 to 5.0, in steps of 0.5, while the multiplicity cut is fixed.

2. *Tag requirements and results*

Events are tagged as $b\bar{b}$'s by requiring at least three quality tracks in the event to have a significance of $\delta_{\rm norm} > 3.0$. These cuts are selected to minimize the overall uncertainty in R_b. Figure 6 shows the b-tagging efficiencies and purities for various normalized impact parameter cuts. The number of events versus the number of quality tracks with $\delta_{\rm norm} > 3.0$ is shown in Fig. 7(a). In the 1993 (1992) data 2617 (815) events are tagged. The results are

	ϵ_b (%)	ϵ_c (%)	ϵ_{uds} (%)	Π_b (%)	$R_b\pm$(statistical error)
1993	62.7	8.9	0.3	89	0.230±0.005
1992	61.7	9.1	0.2	89	0.230±0.009

B. 3D impact parameter method

The 3D impact parameter method explores the full capability of the SLD high precision vertex detector. By using the full 3D information from each track in an event this method is more efficient in tagging b events for the same b purity.

1. *Differences from 2D impact parameter tag method*

The implementation of the 3D impact parameter method differs in only a few respects from that of the

2D impact parameter method. The major difference is that a true 3D impact parameter is calculated for each track from the point on the extrapolated track which minimizes the distance between the track and the PV. This point on the track is referred to as the 3D point of closest approach ($\mathrm{POCA_{3D}}$). The impact parameter is then signed as described in Sec. VII A 1, but using a 3D dot product between the jet direction and the direction of the vector from the PV to the $\mathrm{POCA_{3D}}$. This signed impact parameter is then normalized by the error on the extrapolated track at $\mathrm{POCA_{3D}}$ combined with the beam position error to form $\delta_{3D}^{\mathrm{norm}}$. The distribution of $\delta_{3D}^{\mathrm{norm}}$ compared between data and uncorrected MC simulation is shown in Fig. 5. It should be noted that $\delta_{3D}^{\mathrm{norm}}$ unlike its 2D counterpart (δ_{norm}) has zero phase space at $\delta_{3D}^{\mathrm{norm}} = 0$ leading to the dip visible in Fig. 5. The criteria used for track selection differ from the standard cuts only in that the 3D impact parameter errors and 3D impact parameters are used rather than the xy projection.

2. *Tag requirements and results*

Events are tagged as $b\bar{b}$'s by requiring at least three quality tracks in the event to have a significance of $\delta_{3D}^{\mathrm{norm}} > 3.0$. Figure 6 shows the b-tagging efficiencies and purities for various normalized impact parameter cuts. The number of events versus number of quality tracks with $\delta_{3D}^{\mathrm{norm}} > 3.0$ is shown in Fig. 7(b). In the 1993 (1992) data 3314 (1051) events are tagged. The results are

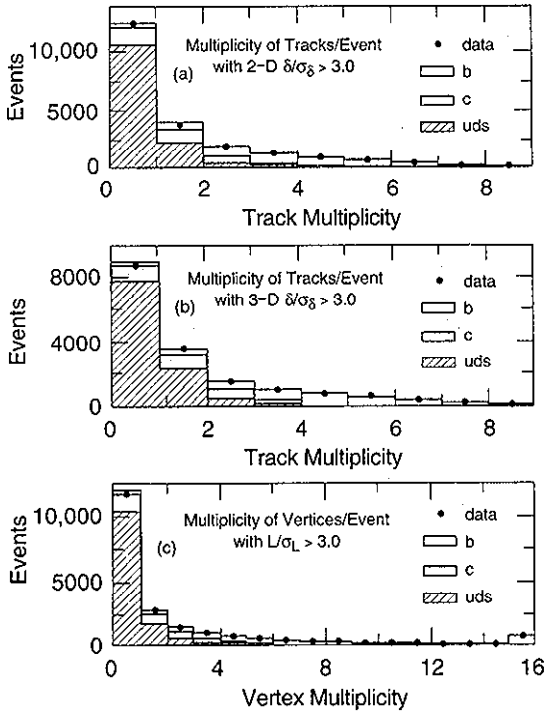

FIG. 7. Data and Monte Carlo event counts vs number of significant tracks and vertices in the events. The Monte Carlo total event count has been normalized to data.

	ϵ_b (%)	ϵ_c (%)	ϵ_{uds} (%)	Π_b (%)	$R_b\pm$(statistical error)
1993	76.7	14.8	0.7	85	0.227±0.004
1992	73.6	14.1	0.6	85	0.240±0.008

C. 3D displaced vertex method

The 3D displaced vertex method exploits the fact that most B decay tracks should form good secondary vertices in 3D to reduce contamination from poorly measured tracks. The large separation of the secondary vertices from the PV reduces sensitivities on errors in the PV position and sensitivities to uncertainties in B lifetimes. The vertex momentum vector provides an estimate of the B momentum direction without relying on an accurate knowledge of the jet direction.

1. *Vertex identification and normalized decay length determination*

All combinations of quality track pairs in the same jet are tested for a 3D geometrical vertex fit. The same jet finding algorithm as that for the impact parameter tag methods is used. The quality track selection differs from the standard cuts only in that the V^0 track rejection is not applied in this analysis. To qualify as an "analysis vertex," the 3D vertex fit χ^2 must be less than 10 and the two-track momentum vector opening angle is required to be $< 90°$ in 3D and $< 160°$ in the $r\phi$ projection. The vertex position $r\phi$ radius is required to be < 2.2 cm to avoid vertices from interactions occurring at the beam pipe and detector material. There are on average ~23 such two-prong analysis vertices per event passing the vertex selection cuts. The MC average event vertex multiplicity with tracking efficiency corrections agrees with the data to ±0.5 vertices. These two-prong vertices are subsequently analyzed individually and no attempt is made to merge them into unique multiple-prong vertices; hence, each track may appear in more than one vertex.

The two-prong vertex decay length (L) is defined as $L = (\vec{r}_v - \vec{r}_0) \cdot \vec{P}_v / |\vec{P}_v|$ where $\vec{r}_v$ is the vertex 3D position vector and $\vec{r}_0$ is the PV position. $\vec{P}_v$ is the summed momentum vector of the two-prong vertex. The projection of the apparent vertex displacement vector to the summed momentum direction helps to suppress effect of spurious track combinations and the effect of a shift in the estimated PV from its true location. This also naturally defines the sign of the decay length as positive if the vertex displacement direction is in the same direction as the vertex momentum vector. The significance is given be the normalized decay length (L_{norm}) which is formed by dividing L by the vertex decay length error, σ_L, where σ_L is obtained from the vertex position error and the PV position error projected along the vertex momentum direction then added in quadrature. The distribution of the normalized decay length compared between the data and uncorrected MC simulation is shown in Fig. 5.

2. Tag requirements and results

Events are tagged as $b\bar{b}$'s by requiring at least four analysis vertices with $L_{\rm norm} > 3.0$. Efficiencies and purities obtained with the b tag for various normalized decay length and vertex multiplicity cuts are shown in Fig. 6. In the 1993 (1992) data 3218 (971) events are tagged. The distribution of the number of analysis vertices with $L_{\rm norm} > 3.0$ in an event is shown in Fig. 7(c) for the data and MC simulation. The results are

	ϵ_b (%)	ϵ_c (%)	ϵ_{uds} (%)	Π_b (%)	$R_b\pm$(statistical error)
1993	71.6	17.6	1.8	79	0.221±0.005
1992	69.1	14.9	1.4	81	0.228±0.009

VIII. SYSTEMATICS

A. Detector systematics

The tracking efficiency systematic reflects the uncertainty in the corrections applied to the MC simulation to obtain the correct yield of quality tracks. To estimate the systematic error associated with the $p_\perp$, ϕ, and $\cos\theta$ dependences of the track efficiency corrections, the change in R_b when it is remeasured with these dependences averaged out relative to the nominal R_b result is used. The observed change is $\sim 1\%$, for all methods, and is taken as the systematic contribution. In addition, a variation of 0.3 tracks per event between different periods of the data is unexplained by the known deficiencies in the MC simulation. Changes in R_b due to a ± 0.3 quality track event multiplicity variation in the MC simulation are included as a systematic error.

The tracking resolution systematic comes from the various corrections to the impact parameters in the MC simulation. These include the $r\phi$ impact parameter modifications to correct for the MC VXD CCD position oversmearing and the rz smearing and shift corrections, as explained in Sec. VI C 2, which predominantly affect only the core of the impact parameter and decay length distributions. The uncertainty is taken as the changes in R_b, that result from not applying these corrections in turn, added in quadrature.

The uncertainty of the primary vertex xy location simulation is represented by adding an $\langle$IP$\rangle$ tail with IP extent of 100 μm for $< 0.25\%$ ($< 0.5\%$) of the 1993 (1992) MC events. The change in R_b that results by adding this tail to the $\langle$IP$\rangle$ position is taken as the systematic from the modeling of the precision to which the $\langle$IP$\rangle$ is tracked. In both the 3D impact parameter tag and the 3D displaced vertex tag the MC events with PV z greater than 100 μm from the true MC event PV z have their weights increased by 50% to conservatively estimate the contribution from unmodeled PV z tails.

The MC statistical error on the trigger and event selection flavor bias is also taken as a systematic error. The combined detector and IP modeling uncertainties for each method are shown in Table III.

B. Physics systematics

Systematics due to the uncertainty of physics quantities in the MC simulation are estimated using a MC event weighting technique. The MC event weights are assigned according to the probability ratio between the

TABLE III. Summary of detector and physics systematics for each $b\bar{b}$-tagging method.

Detector Modeling	2D Impact error (%)	3D Impact error (%)	3D Vertex error (%)
Tracking/linking efficiency	2.9	2.5	4.9
Tracking resolution	0.5	1.5	1.3
Beam position tails	0.5	0.5	0.3
Trigger/event selection	0.5	0.5	0.5
Subtotal	3.1	3.1	5.1
Physics Modeling	**2D Impact error (%)**	**3D Impact error (%)**	**3D Vertex error (%)**
B lifetimes ($\tau_{B\ \rm meson} = 1.55 \pm 0.10$ ps, $\tau_{B\ \rm baryon} = 1.10 \pm 0.30$ ps)	2.6	1.4	1.2
b fragmentation (Peterson $\langle x_e\rangle = 0.695 \pm 0.021$)	2.2	1.2	0.8
b fragmentation (Bowler vs Peterson w/$\langle x_e\rangle = 0.695$)	0.2	0.8	0.6
b baryon production ($8.9 \pm 3.0\%$)	0.6	0.5	0.7
B decay to D^+ ($\pm 6\%$ absolute)	0.3	0.3	0.4
B decay multiplicity (± 0.25 tracks per B decay)	2.2	1.5	3.6
B model (exclusive phase space vs tuned LUND 6.3)	0.7	1.0	1.0
c fragmentation (Peterson $\langle x_e\rangle$ for $D^* = 0.501 \pm 0.025$)	0.5	0.4	0.2
c fragmentation (Bowler vs Peterson w/$\langle x_e\rangle = 0.501$)	0.1	0.1	0.2
c decay to D^+ ($\pm 5\%$ absolute)	<0.1	0.7	0.6
c decay multiplicity	0.9	0.8	1.5
s production ($s\bar{s}$ popping varied by 10%)	0.3	0.1	0.2
uds decay multiplicity (± 0.3 tracks)	0.1	0.1	0.2
$g \to b\bar{b}$ splitting($\pm 50\%$)	0.5	0.5	0.2
$g \to c\bar{c}$ splitting($\pm 50\%$)	0.3	0.3	0.2
$\Gamma(Z^0 \to c\bar{c})$ ($R_c = 0.171 \pm 0.017$)	1.0	1.4	1.7
Jet axis modeling (JADE $y_{\rm cut}$ varied from 0.01 to 0.10)	0.8	0.8	0.8
Subtotal	4.4	3.3	4.8
Total	5.4	4.6	6.9

nominal MC distribution and an alternative distribution which represents the uncertainty for a physics variable. Using the event weighting scheme the following physics systematics are studied.

The average B hadron lifetime is varied by ± 0.10 ps for B mesons and ± 0.30 ps for B baryons. These variations are based on the current exclusive B lifetime measurement errors which are generous given the constraint of the more precisely known average B hadron lifetime [36]. The effect of uncertainty in heavy flavor fragmentation is determined by varying the ϵ parameter of the Peterson fragmentation function to correspond to $\delta\langle x_E\rangle = \pm 0.025$ and ± 0.021 for c and b quarks, respectively. These variations are conservative choices, larger than the error on some of the individual measurements [22], chosen because of our rather indirect knowledge of the complex fragmentation process. In addition, results derived from the modified Bowler fragmentation function [39] for c and b quarks, with a significantly different fragmentation function shape, are compared with the results obtained using the Peterson function for the same $\langle x_E\rangle$. The mean charged multiplicity per B hadron decay is varied by ± 0.25 tracks. This corresponds to a $\sim 2\sigma$ error on B meson decay average charged multiplicity measured at the $\Upsilon(4s)$ [33,34]. The choice of this large variation is aimed at covering the lack of knowledge on B_s and B baryon decay multiplicities. A 6% absolute variation is applied to the B decay D^+ production ratio $\frac{\Gamma(B\to D^+X)}{\Gamma(B\to \mathrm{all})}$ due to the distinctly long lifetime of the D^+ compared to other charm hadrons. The generous variation on this ratio compared to present experimental uncertainty of $\pm 4\%$ [36] is taken as a representative estimate covering uncertainties in the production of all charmed hadron species in B hadron decays. The effect of varying the B baryon production rate in $b\bar{b}$ events by 3% is also examined in view of its different lifetime compared to the B mesons. To estimate the effect of the details of the kinematics in the B decay model, an MC $b\bar{b}$ event sample with an alternative B decay model is used. This alternative model is also tuned to the various measurements at $\Upsilon(4s)$ but the decay product momenta for hadronic B decay modes are distributed by pure phase space. The charm hadron decay mean charged multiplicities are varied by ± 0.06, ± 0.10, ± 0.31, and ± 0.40 for D^0, D^+, D_s, and Λ_c, respectively. The uncertainties assigned to the D^0 and D_s decay charged multiplicities are according to the Mark III measurement [25] while the uncertainty for D^+ is taken as the discrepancy between the MC and MARK III measurement mainly due a deficit of one-prong D^+ decay modes in the MC simulation. These charmed hadron decay multiplicity variations are applied to $b\bar{b}$ as well as $c\bar{c}$ events in the determination of R_b variations. A variation of $\pm 5\%$ in the D^+ production rate in $c\bar{c}$ events is used as a representative systematic of the production rate uncertainties of various charmed hadron species. The production of long-lived strange particles in the fragmentation process can be a significant cause of tagging the light flavor events. This effect is studied from the event fragmentation K^0 and Λ production multiplicity by varying the MC fragmentation $s\bar{s}$ popping suppression factor relative to $u\bar{u}$ and $d\bar{d}$ popping in the range 0.30 ± 0.03. The influence due to the uncertainty associated with the fragmentation of uds events is checked further by a variation of the average event charged multiplicity by ± 0.3 tracks for uds events corresponding to the typical measurement error of the event mean charged multiplicity for all $Z^0 \to$ hadrons events [23]. Finally, a crude estimate is made for the effect of heavy quark pair production due to gluon splitting. This is done by simply varying the $g \to b\bar{b}$ and $g \to c\bar{c}$ rates by 50% from that predicted by JETSET.

In addition, the effect of the present experimental uncertainty in the $Z^0 \to c\bar{c}$ branching fraction of $\delta R_c = \pm 0.017$ is also included as a systematic error as it is used directly in the R_b calculation. The uncertainty introduced by MC jet axis modeling is determined by varying the JADE jet finding algorithm parameter y_{cut} from 0.01 to 0.10. The resulting effect of each physics systematic on R_b for each $b\bar{b}$-tagging method is given in Table III where the subtotal is obtained from summing the contributions in quadrature.

The different tagging methods clearly have different sensitivities to different systematics despite all being lifetime tags. It can be seen from Table III that the 2D impact parameter tag is more sensitive to the B lifetime uncertainty due to the less distinctive decay lifetime information in a projective view. The displaced vertex tag is on the other hand more sensitive to decay multiplicity uncertainties and tracking inefficiencies, an understood feature due to the amplified track pair combinatorial fluctuation with track multiplicity. The 3D impact parameter tag with a more evenly distributed systematics is giving the lowest overall systematic error. A common feature between the three methods is that the bulk of the systematics on R_b come from the uncertainty on the b-tagging efficiency ϵ_b with origins in both physics and detector simulation.

C. Verifications

The stability of the R_b results are checked for consistency within the estimated errors. All results are checked against variations with the b-tagging cuts. The variations of measured R_b versus track or vertex multiplicity with different significance cuts are shown in Fig. 8. The low multiplicity and low significance regions are more sensitive to $udsc$ background and detector resolution effects while the high multiplicity and high significance regions are more sensitive to b physics systematics and tracking efficiency. The variations of the measured R_b values for the different tagging cuts can be seen to be generally within the total errors at the nominal cuts where the total errors are expected to be smallest.

Variations of the R_b results versus orientation of the events are studied by measuring R_b for events with thrust axis direction in different ϕ regions separately. The ambiguity in the thrust direction is removed by taking the thrust axis to always point along the positron beam direction. The result for each method in each ϕ region is given in Table IV and the results in different ϕ regions

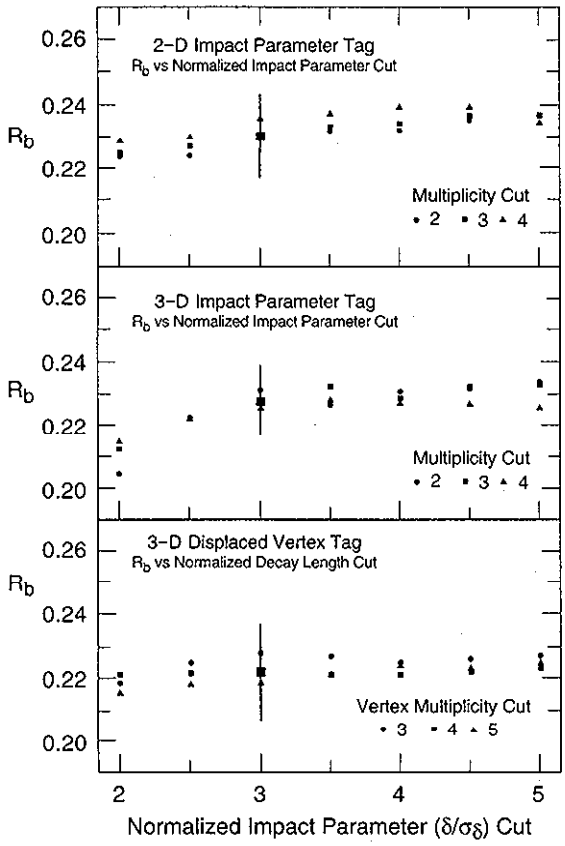

FIG. 8. R_b versus tagging cuts in the 2D and 3D impact tag and the 3D displaced vertex tag. The result at nominal cuts for each method is shown as a large square together with the estimated total error bar at the nominal cuts.

can be seen to be statistically consistent with each other for each method.

The variations of measured R_b can also be checked versus the time periods the data were taken. The results from the 1993 data and 1992 data are statistically consistent with each other for each of the methods as seen from Sec. VII. When the 1993 data is divided into two periods for early and late 1993, the results are again consistent for each of the three methods.

IX. SUMMARY

R_b has been measured at the SLD using three methods with high b-tagging efficiency and purity utilizing the precision vertex detector combined with the small stable SLC interaction point. These measurements yield values of the 2D impact parameter method, $R_b = 0.230 \pm 0.004(\text{stat}) \pm 0.012(\text{syst})$, the 3D impact parameter method, $R_b = 0.230 \pm 0.004(\text{stat}) \pm 0.010(\text{syst})$, and the 3D displaced vertex method, $R_b = 0.223 \pm 0.004(\text{stat}) \pm 0.015(\text{syst})$.

A combined result is made using correlations estimated from the MC simulation according to the method of Lyons *et al.* [40]. The correlation between the 2D impact parameter and 3D impact parameter methods, the 3D impact parameter and 3D displaced vertex methods, and the 2D impact parameter and 3D displaced vertex methods were found to be 78%, 59%, and 68%, respectively. The result is

$$R_b = 0.229 \pm 0.011$$

(combined statistical and systematic error).

In conclusion, we have used three different variations of lifetime b tags to measure R_b, and all give results consistent with the standard model. Currently, our measurement precision has not yet reached the level of being able to probe the details of the $Z^0 \to b\bar{b}$ vertex corrections and discriminate between different models. We have demonstrated that the crucial issue of the precision vertex detector resolution, especially the tails of distributions relevant to the lifetime tagging technique in general, can indeed be brought to a good level of understanding through dedicated detector calibration and detailed MC simulation. Uncertainties due to modeling the detector response are expected to decrease further as tracking inefficiencies are better understood. The dominant contribution to the detector systematics results from the number of tracks per event variation observed between different periods of the data. This is unlikely to enter in the analysis of future SLD runs. The physics modeling systematics are not expected to significantly decrease using these techniques in the near future. However, the simple approach of the event tag analyses with tagging efficiencies from MC simulations has yielded much detailed knowledge of the physics modeling and detector simulation issues associated with the lifetime b-tagging techniques through a direct confrontation with these sensitive issues. This provides a solid foundation for development of techniques with lower systematic errors, leading to higher precision R_b measurements.

TABLE IV. R_b results versus axial quadrants of the SLD. The errors are statistical only.

SLD ϕ Quadrant	2D impact R_b	3D impact R_b	3D vertex R_b
$\frac{-\pi}{4} < \phi < \frac{\pi}{4}$	0.234 ± 0.009	0.232 ± 0.008	0.226 ± 0.009
$\frac{\pi}{4} < \phi < \frac{3\pi}{4}$	0.231 ± 0.009	0.236 ± 0.008	0.230 ± 0.009
$\frac{3\pi}{4} < \phi < \frac{5\pi}{4}$	0.230 ± 0.009	0.225 ± 0.008	0.228 ± 0.009
$\frac{5\pi}{4} < \phi < \frac{-\pi}{4}$	0.225 ± 0.009	0.216 ± 0.008	0.212 ± 0.009

ACKNOWLEDGMENTS

We thank the staff of the SLC for their efforts in the challenging task of bringing submicrometer-sized stable colliding beams to the SLD for a unique physics program. We thank the technical staff at the collaborating institutions for their valiant support in the construction and maintenance of the SLD. This work was supported by Department of Energy Contracts Nos. DE-FG02-91ER40676 (BU), DE-FG03-92ER40701 (CIT), DE-FG03-91ER40618 (UCSB),

DE-FG03-92ER40689 (UCSC), DE-FG03-93ER40788 (CSU), DE-FG02-91ER40672 (Colorado), DE-FG02-91ER40677 (Illinois), DE-AC03-76SF00098 (LBL), DE-FG02-92ER40715 (Massachusetts), DE-AC02-76ER03069 (MIT), DE-FG06-85ER40224 (Oregon), DE-AC03-76SF00515 (SLAC), DE-FG05-91ER40627 (Tennessee), DE-AC02-76ER00881 (Wisconsin), DE-FG02-92ER40704 (Yale); National Science Foundation grants: PHY-91-13428 (UCSC), PHY-89-21320 (Columbia), PHY-92-04239 (Cincinnati), PHY-88-17930 (Rutgers), PHY-88-19316 (Vanderbilt), PHY-92-03212 (Washington); the UK Science and Engineering Research Council (Brunel and RAL); the Istituto Nazionale di Fisica Nucleare of Italy (Bologna, Ferrara, Frascati, Pisa, Padova, Perugia); and the Japan-US Cooperative Research Project on High Energy Physics (Nagoya, Tohoku).

[1] A. Akhundov, D. Bardin, and T. Riemann, Nucl. Phys. **B276**, 1 (1986); W. Beenakker and W. Hollik, Z. Phys. C **40**, 141 (1988); B. W. Lynn and R. G. Stuart, Phys. Lett. B **252**, 676 (1990); J. Bernabéu, A. Pich, and A. Santamaria, *ibid.* **363**, 326 (1991).

[2] CDF Collaboration, F. Abe *et al.*, Phys. Rev. Lett. **74**, 2626 (1995); D0 Collaboration, S. Abachi *et al.*, *ibid.* **74**, 2632 (1995).

[3] W. Hollik, Mod. Phys. Lett. A **5**, 1909 (1990); F. Boudjema, A. Djouadi, and C. Verzegnassi, Phys. Lett. B **238**, 423 (1990); A. Djouadi *et al.*, Nucl. Phys. **B349**, 48 (1991); M. Boulware and D. Finnel, Phys. Rev. D **44**, 2054 (1991); R. S. Chivukula, E. H. Simmons, and J. Terning, Phys. Lett. B **331**, 383 (1994).

[4] T. Liu and D. Ng, Phys. Lett. B **342**, 262 (1995).

[5] ALEPH Collaboration, D. Buskulic *et al.*, Z. Phys. C **62**, 179 (1994); DELPHI Collaboration, P. Abreu *et al.*, *ibid.* **56**, 63 (1992); L3 Collaboration, B. Adeva *et al.*, Phys. Lett. B **259**, 199 (1991), OPAL Collaboration, P. D. Acton *et al.*, Z. Phys. C **58**, 523 (1993).

[6] DELPHI Collaboration, P. Abreu *et al.*, Phys. Lett. B **281**, 383 (1992).

[7] ALEPH Collaboration, D. Buskulic *et al.*, Phys. Lett. B **313**, 535 (1993); OPAL Collaboration, P. D. Acton *et al.*, Z. Phys. C **60**, 579 (1993); OPAL Collaboration, D. Akers *et al.*, *ibid.* **65**, 17 (1994); DELPHI Collaboration, P. Abreu *et al.*, *ibid.* **65**, 555 (1995).

[8] ALEPH Collaboration, D. Buskulic *et al.*, Phys. Lett. B **313**, 549 (1993); DELPHI Collaboration, P. Abreu *et al.*, *ibid.* **295**, 383 (1992); L3 Collaboration, O. Adriani *et al.*, *ibid.* **307**, 237 (1993); OPAL Collaboration, R. Akers *et al.*, Z. Phys. C **61**, 357 (1994).

[9] SLD Collaboration, G. Agnew *et al.*, SLD Design Report SLAC-0273, 1984 (unpublished).

[10] TASSO Collaboration, W. Braunschweig *et al.*, Z. Phys. C **38**, 543 (1988).

[11] MARK-II Collaboration, R. Jacobsen *et al.*, Phys. Rev. Lett. **67**, 3347 (1991).

[12] G. Agnew *et al.*, in *Proceedings of the 26th International Conference on High Energy Physics*, Dallas, Texas, 1992, edited by J. Sanford, AIP Conf. Proc. No. 272 (AIP, New York, 1993).

[13] M. Hildreth *et al.*, in *1994 IEEE Conference record*, Proceedings of the Nuclear Science Symposium and Medical Imaging Conference, Norfolk, Virginia, edited by R. C. Tredler (IEEE, New York, 1994).

[14] D. Axen *et al.*, Nucl. Instrum. Methods A **328**, 472 (1993).

[15] P. Billoir, Nucl. Instrum. Methods **225**, 352 (1984).

[16] D. Williams, Ph.D. thesis, MIT, 1994.

[17] R. Cotton, Ph.D. thesis, Brunel University, 1993.

[18] T. Sjöstrand and M. Bengtsson, Comput. Phys. Commum. **43**, 367 (1987); T. Sjöstrand, *ibid.* **39**, 347 (1986).

[19] TASSO Collaboration, W. Braunschweig *et al.*, Z. Phys. C **41**, 359 (1988); P. N. Burrows, *ibid.* **41**, 375 (1988).

[20] OPAL Collaboration, M. Z. Akrawy *et al.*, Z. Phys. C **47**, 505 (1990).

[21] C. Peterson *et al.*, Phys. Rev. D **27**, 105 (1983).

[22] ALEPH Collaboration, D. Buskulic *et al.*, Z. Phys. C **62**, 179 (1994); L3 Collaboration, B. Adeva *et al.*, Phys. Lett. B **261**, 177 (1991); OPAL Collaboration, R. Akers *et al.*, Z. Phys. C **60**, 199 (1993); OPAL Collaboration, R. Akers *et al.*, *ibid.* **61**, 209 (1994); ALEPH Collaboration, D. Buskulic *et al.*, *ibid.* **62**, 1 (1994); DELPHI Collaboration, P. Abreu *et al.*, *ibid.* **59**, 533 (1993); OPAL Collaboration, R. Akers *et al.*, *ibid.* **60**, 601 (1993).

[23] ALEPH Collaboration, D. Decamp *et al.*, Phys. Lett. B **273**, 181 (1991); DELPHI Collaboration, P. Abreu *et al.*, Z. Phys. C **50**, 185 (1991); L3 Collaboration, B. Adeva *et al.*, Phys. Lett. B **259**, 199 (1991); OPAL Collaboration, P. D. Acton *et al.*, Z. Phys. C **53**, 539 (1992).

[24] Particle Data Group, K. Hikasa *et al.*, Phys. Rev. D **45**, S1 (1992).

[25] MARK III Collaboration, D. Coffman *et al.*, Phys. Lett. B **263**, 135 (1991).

[26] M. Wirbel, B. Stech, and M. Bauer, Z. Phys. C **29**, 637 (1985).

[27] CLEO Collaboration, F. Butler *et al*, Phys. Rev. Lett. **69**, 2041 (1992).

[28] N. Isgur, D. Scora, B. Grinstein, and M. B. Wise, Phys. Rev. D **39**, 799 (1989); code provided by P. Kim and CLEO Collaboration,

[29] CLEO Collaboration, M. Artuso, in *Proceedings of the Workshop on B Physics at Hadron Accelerators*, Snowmass, Colorado, 1993, edited by C. Shekhar Mishra and Patricia McBride (Fermilab, Batavia, 1994).

[30] CLEO Collaboration, G. Crawford *et al.*, Phys. Rev. D **45**, 752 (1992).

[31] M. Thulasidas, Ph.D thesis, Syracuse University, 1993.

[32] CLEO Collaboration, F. Muheim in *The Albuquerque Meeting*, Proceedings of the Meeting of the Division of Particles and Fields of the APS, Albuquerque, New Mexico, 1994, edited by S. Seidel (World Scientific, Singapore, 1995).

[33] ARGUS Collaboration, H. Albrecht *et al.*, Z. Phys. C **54**, 13 (1992).

[34] CLEO Collaboration, R. Giles *et al*, Phys. Rev. D **30**, 2279 (1984).

[35] ARGUS Collaboration, H. Albrecht *et al.*, Z. Phys. C **58**, 191 (1993); ARGUS Collaboration, H. Albrecht *et al.*,

ibid. **62**, 371 (1994).
[36] The Particle Data Group, L. Montanet *et al.*, Phys. Rev. D **50**, 1173 (1994).
[37] Computer code GEANT 3.15, CERN Application Software Group, **CERN Program Library** (1993).
[38] JADE Collaboration, S. Bethke *et al.*, Phys. Lett. B **213**, 235 (1988).
[39] M. G. Bowler, Z. Phys. C **11**, 169 (1981); T. Sjöstrand, Comput. Phys. Commun. **82**, 74 (1994).
[40] L. Lyons *et al.*, Nucl. Instrum Methods A **270**, 110 (1988).